International Journal of Heat and Mass Transfer 52 (2009) 3929–3942

Contents lists available at ScienceDirect

International Journal of Heat and Mass Transfer

journal homepage: www.elsevier.com/locate/ijhmt

# Computational optimization of the thermal performance of internally finned ducts

Eric Duplain, B. Rabi Baliga *

*Heat Transfer Laboratory, Department of Mechanical Engineering, McGill University, 817 Sherbrooke St. W., McGill University, Montreal, Quebec, Canada H3A 2K6*

ARTICLE INFO

*Article history:*
Received 1 December 2008
Accepted 23 March 2009
Available online 6 May 2009

*Keywords:*
Internally finned ducts
Conjugate heat transfer
Thermal performance
Non-uniform rational B-splines
Fin shape
Optimization
Gradient method
Newtonian fluid
Quasi one-dimensional fin equation
Control-volume finite element method
Finite volume method

ABSTRACT

A computational methodology for optimization of fin shapes is formulated and demonstrated in the context of steady, laminar, fully-developed forced convection in a straight duct of circular cross-section, with air as the fluid and non-twisted, uninterrupted, longitudinal internal fins made of steel, aluminium, and copper. The governing equations are solved using finite volume methods. The fins shapes are approximated using non-uniform rational B-splines, with the control points as design variables. A gradient-based method is used for the optimization. Results pertaining to the maximization of suitably defined thermal performance, subject to constant pumping power per unit length, are presented and discussed.



## 1. Introduction

A computational methodology for the optimization of conjugate convective and conductive heat transfer in internally finned ducts is formulated and demonstrated in this paper. The particular optimization criterion used is the maximization of the thermal performance for a fixed specified value of the pumping power per unit length. However, the proposed methodology can be adapted to work with other suitable optimization criteria. In internally finned ducts, the pumping power needed to achieve the desired rate of fluid flow is influenced by the following parameters: number, base thickness, height (or length), and shape of the fins; shape and other geometric parameters of the flow passage; and thermofluid properties of the fluid. These parameters, as well as the thermal conductivities of the fin material and fluid, and the thermal boundary conditions influence the rate of heat transfer from the internally finned duct to the fluid, or vice versa. Hence, all combinations of these parameters must be explored to find one that meets the specified thermal optimization criterion.

Internal fins are routinely used to enhance heat transfer in ducts encountered in a wide variety of energy conversion, exchange, and storage equipment used in the chemical, aeronautical, automotive, and heating, ventilating and air-conditioning (HVAC) industries, as is discussed in the works of Kays and London [1], Hesselgreaves [2], and Shah et al. [3]. They are also used in recuperators of industrial gas turbine engines, cooling systems for electronics, thermal and nuclear power plants, and biomedical equipment [1–4]. Bergles [4] has reviewed the historical background, driving trends, and benefits of numerous heat transfer enhancement techniques, and stated that analytical or numerical prediction techniques should be used to effectively develop improved heat transfer surfaces. Based on these observations, it may be concluded that a relatively simple-to-implement and cost-effective computational methodology for the optimization of the thermal performance of internally finned ducts could yield a wide range of benefits.

Examples of computational investigations of fluid flow and heat transfer in a variety of plate-fin ducts include the works of Sparrow et al. [5], Patankar et al. [6], Patankar and Prakash [7], Kelkar and Patankar [8], Amon et al. [9], Suzuki et al. [10], Zhang et al. [11], Acharya et al. [12], DeJong et al. [13], Saidi and Sundén [14], Shah et al. [3], and Lamoureux and Baliga [15], among others. The works of Masliyah and Nandkumar [16] and Soliman et al. [17] are examples of some early computational investigations of laminar, fully-developed, forced convection in straight tubes (of circular cross-section) with internal fins of triangular cross-section. Patankar et al. [18] used a mixing-length model and a finite volume method to analyze fully-developed turbulent flow and heat transfer in tubes and annuli with longitudinal internal fins. Webb and Scott [19] have conducted a parametric analysis of forced convection in internally finned tubes. Baliga and Azrak [20] have determined the characteristics of laminar fully-developed flow and heat

* Corresponding author. Fax: +1 514 398 4476.
*E-mail address:* bantwal.baliga@mcgill.ca (B.R. Baliga).

0017-9310/$ - see front matter © 2009 Elsevier Ltd. All rights reserved.
doi:10.1016/j.ijheatmasstransfer.2009.03.030

**Nomenclature**

| | |
|---|---|
| $A_{c\text{-}s}$ | cross-sectional area available for fluid flow in the ducts |
| **C** | NURBS curve vector |
| $c_p$ | specific heat at constant pressure |
| $D_h$ | hydraulic diameter |
| $f(\mathbf{X})$ | objective function |
| $f_{Darcy}$ | Darcy friction factor |
| $g(\mathbf{X})$ | constraint function |
| $h$ | control point height above the fin symmetry plane |
| $h_{av}$ | average heat transfer coefficient |
| $k$ | thermal conductivity |
| $l^*$ | normalized fin length |
| $l_f$ | fin length |
| $N_{i,p}$ | NURBS basis function of $p$th degree associated with control point $i$ |
| $n_{fin}$ | number of fins |
| $Nu$ | Nusselt number |
| $p$ | static pressure |
| $P$ | reduced pressure |
| **P** | vector of NURBS control points |
| $Peri_{wetted}$ | wetted perimeter of $A_{c\text{-}s}$ |
| $pp$ | pumping power per unit length |
| $pp_{target}$ | target (desired) pumping power per unit length |
| $Pr$ | Prandtl number |
| $q'$ | rate of heat input per unit axial length of duct |
| $r$ | radius of the circular cross-section of the duct |
| $Re$ | Reynolds number |
| **S** | normalized search-direction vector |
| $T$ | temperature |
| $u, v$ | velocity components in the $x$ and $y$ directions, respectively |
| **U** | NURBS knot vector |
| $w$ | axial velocity component |
| $W$ | dimensionless axial velocity component |
| $x$ | Cartesian coordinate |
| $X$ | dimensionless Cartesian coordinate |
| **X** | design vector |
| $y$ | Cartesian coordinate |
| $Y$ | dimensionless Cartesian coordinate |
| $z$ | Cartesian coordinate along the axial direction |
| $z^*$ | dimensionless Cartesian coordinate along the axial direction |

*Greek letters*

| | |
|---|---|
| $\Delta$ | fin thickness |
| $\varepsilon$ | convergence criterion |
| $\Xi$ | dimensionless coordinate along the centerline of the fin |
| $\eta^{(H)}$, $\eta^{(T)}$ | thermal performance enhancement indices for the (H) and (T) boundary conditions |
| $\theta$ | dimensionless temperature for the (H) thermal boundary condition |
| $\lambda$ | step size |
| $\mu$ | dynamic viscosity of the fluid |
| $\rho$ | density of the fluid |
| $\sigma$ | half-angle of the fin base |
| $\varphi$ | dimensionless temperature for the (T) thermal boundary condition |
| $\Omega$ | local fin conductance |

*Subscripts*

| | |
|---|---|
| $av$ | average value |
| $b$ | bulk value |
| $f$ | fluid |
| $fin$ | pertaining to the fin |
| $w$ | pertaining to the duct wall |
| $\perp$ | perpendicular or normal component |

*Superscripts*

| | |
|---|---|
| (H) | pertaining to the thermal boundary condition involving uniform heat input per unit axial length and uniform duct wall temperature in any cross-section |
| (T) | pertaining to the thermal boundary condition involving constant duct wall temperature, axially and peripherally |

transfer in straight, uninterrupted, plate-fin ducts of triangular cross-section. Zhang and Faghri [21] have conducted a numerical study of internally finned tubes for applications in latent heat thermal energy storage systems. Heat transfer enhancement using fins in the microscale regime for applications in electronics has been investigated by Chou et al. [22]. The aforementioned studies have improved the understanding of fluid flow and heat transfer in internally finned ducts, and also elucidated the mechanisms responsible for enhancements of the rates of heat transfer relative to those in ducts without internal fins. However, no efforts were made in these studies to specifically optimize the thermal performance of these internally finned ducts.

Optimization techniques in engineering started to become increasingly well-established and used in the late 1950s, with the advent of digital computers. Over the last two decades, several publications have focused on overall reviews, recent advances, and specific applications of optimization techniques such as the Simplex, gradient-based, Lagrange multiplier, and evolutionary or genetic algorithms, and also constructal theory. Examples of such publications include the works of Pironneau [23], Rao [24], Jameson et al. [25], Fabri [26,27], Bejan [28], Deb [29], Onwubolu and Babu [30], Mohammadi and Pironneau [31], Bobaru and Rachakonda [32,33], Bejan and Lorente [34], Dias and Milanez [35], Hilbert et al. [36], Lorenzini and Rocha [37], Duvigneau et al. [38], Janiga [39], Tye-Gingras and Gosselin [40], Shinohara et al. [41], and da Silva and Gosselin [42]. A related topic, which also has very useful applications in engineering, is the solution of inverse heat transfer problems, where the objective is to obtain a design that produces desired measurements or results as precisely as possible. This topic is covered in the works of Kurpisz and Nowak [43], Özisik and Orlande [44], and Ashrafizadeh et al. [45,46], among others.

Constructal theory has been used to optimize assemblies or arrays of fins of fixed geometrical shapes, such as T- and Y-shaped fins in the work of Lorenzini and Rocha [37], for example. The optimized arrays or assemblies have fractal like features, akin to those displayed by natural flow structures [28,34]. There have also been studies on the optimal spacing between fins of fixed rectangular shape on a vertical wall under natural convection conditions, such as those in the works of Bar-Cohen [47] and Bar-Cohen and Rohsenow [48], for example. In the work of Razelos and Krikkis [49], a procedure for the optimization of the thermal design of longitudinal fins of rectangular cross-section is presented.

A study by Tsukamoto and Seguchi [50] is among the first ones in which the optimal *shape* of cooling fins is considered. They numerically solved a quasi one-dimensional model of heat conduction in the fin and approximated the fin shape with a second-order polynomial, the coefficients of which were the design variables. More recently, optimization of the shape of convectively cooled fins has been carried out by Bobaru and Rachakonda [32,33] using an element-free Galerkin (EFG) method for the analysis of heat

conduction within the fin. However, they used semi-empirical correlations for calculating the distribution of the heat transfer coefficient on the surface of the fins: this approach may work reasonably well under some conditions of external convection on the surfaces of fins, but it is not well-suited for the thermal optimization of internally finned ducts, for which it is important to solve the conjugate problem of heat conduction within the fin and convection in the fluid [20].

Lorenzini et al. [51] and Fabri [26,27,52,53] have proposed and illustrated the use of genetic algorithms for optimizing the shape of fins attached to planar surfaces, in the context of fully-developed laminar flow. In these studies, the fin surface was approximated by a polynomial, and the design variables were the polynomial coefficients. They found that the optimal fins have undulated or rippled shapes, and the number and size of the undulations and also the increase in the fin thermal effectiveness, relative to a reference fin of rectangular shape, depend on the order of the polynomial that is used to approximate the fin profile. It should also be noted that genetic (or evolutionary) algorithms are well-suited for the solution of multi-objective optimization problems and operate on the entire allowed design space, but they require a large number of simulations and thus have a high computational cost. Therefore, though genetic algorithms coupled with computational fluid dynamics methods have been used successfully for the solution of multi-objective optimization problems, they are still not considered as a practical optimization tool for engineering applications [36,39,54].

In the proposed computational methodology for the optimization of internally finned ducts, the shapes of the internal fins are approximated by non-uniform rational B-splines (NURBS) [55], with the control points as design variables, and a two-stage iterative solution technique is used: in the first stage, a control-volume finite element method (CVFEM) [56,57] and a finite volume method (FVM), both inspired by the seminal contributions of Spalding [58], Patankar and Spalding [59], and Patankar [60], are used to solve the so-called *direct* problem, namely, the mathematical models of conjugate convection in the fluid and quasi one-dimensional conduction inside the fins, respectively; in the second stage, an optimization algorithm, based on a gradient approach and inputs from solutions of the aforementioned direct problem, is used to calculate a new geometry of the internally finned duct that moves it towards the desired design. These two stages are used sequentially and repeatedly (iteratively) until the solution is optimal within a specified tolerance. In this context, it should be noted that the gradients required in the optimization algorithm of the proposed methodology may be obtained using either direct numerical differentiation (of results yielded by solutions of the intermediate direct problems), continuous sensitivity equations (CSE), or adjoint methods [25,38,41,61]. The direct numerical differentiation method is computationally expensive, as it requires inputs from several solutions of the direct problem in every step of the overall optimization procedure. However, it is relatively simple to implement. Therefore, it was used to solve the demonstration problem in this work. On the other hand, the CSE and adjoint methods are more challenging to implement correctly, but require relatively lower computing times, if implemented efficiently [25,38,41]: thus, they are recommended for a practical implementation of the proposed computational methodology.

The proposed overall computational methodology does not depend on any specific internally finned duct flow and heat transfer problem. In this paper, it is demonstrated in the context of steady, fully-developed, laminar forced convection in straight ducts of circular cross-section, with non-twisted, continuous, longitudinal fins. Air is the working fluid, and the fin materials explored are stainless steel, aluminium, and copper. The reasons for the choice of this particular demonstration problem are the following: it is conceptually simple, yet practical; the mathematical models for the associated fluid flow and heat transfer are well established; and it provides a relatively convenient and computationally inexpensive way of illustrating the benefits of the proposed optimization methodology.

## 2. Fluid flow and heat transfer in the demonstration problem: mathematical models and numerical solution methods

A representative cross-section of the internally finned ducts considered in the demonstration problem is schematically illustrated in Fig. 1. The fins shown in this figure are of triangular cross-section, but the shape of the fin cross-section in the optimized ducts can be quite different. The equations and boundary conditions that govern the fluid flow and heat transfer phenomena in this problem are presented first in the context of the following assumptions: (i) in the range of operation considered, the fluid (air) behaves as a Newtonian fluid, and the thermophysical properties of this fluid and also those of the fin material (pegged to average values) are essentially constant; (ii) in the axial direction, heat conduction inside the fluid, duct wall, and fins is negligible compared to advection in this direction and conduction in the radial direction; (iii) viscous dissipation in the fluid is negligible; (iv) steady, fully-developed, laminar fluid flow and heat transfer prevail; and (v) in the duct cross-section, with air as the working fluid, metal fins (stainless steel, aluminum, and copper), and the geometric parameters investigated, heat conduction inside each fin is essentially quasi one-dimensional in the direction of its centerline [20,62,63]. Following the presentation of these mathematical models, synopses of the numerical methods that were used to solve them are presented.

### 2.1. Equations governing the fluid flow

With respect to the cross-section of the internally finned duct and the Cartesian coordinate system depicted in Fig. 1, and in the context of the above-mentioned assumptions, in the fully-developed flow region, the velocity components in the $x$ and $y$ directions are zero ($u = v = 0$), the velocity component in the $z$ direction, $w$, is a function of $x$ and $y$ only (independent of $z$, as indicated by the continuity equation, $\partial w/\partial z = 0$), and the $z$-momentum equation reduces to the following form [64,65]:

$$0 = -\frac{\partial p}{\partial z} + \rho g_z + \frac{\partial}{\partial x}\left(\mu\frac{\partial w}{\partial x}\right) + \frac{\partial}{\partial y}\left(\mu\frac{\partial w}{\partial y}\right) = -\frac{dP}{dz} + \frac{\partial}{\partial x}\left(\mu\frac{\partial w}{\partial x}\right) + \frac{\partial}{\partial y}\left(\mu\frac{\partial w}{\partial y}\right)$$
$$P \triangleq p - \rho g_x x - \rho g_y y - \rho g_z z \tag{1}$$

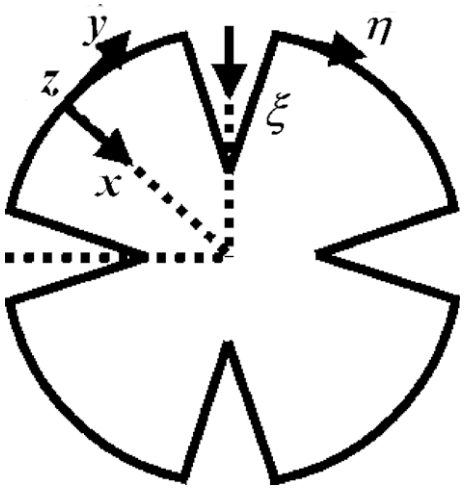


**Fig. 1.** Representative cross-section of an internally finned duct and the coordinate systems used in the mathematical models.

In this equation, $p$ is the static pressure; $\rho$ and $\mu$ are the density and dynamic viscosity of the fluid, respectively; $g_x$, $g_y$, and $g_z$ are the $x$, $y$, and $z$ components, respectively, of the gravitational acceleration vector; and $P$ is the reduced pressure [64]. In the fully developed region, the reduced pressure, $P$, is constant in any cross-sectional plane of the duct and drops linearly with $z$ [64,65]: $-dP/dz$ = constant > 0.

### 2.2. Energy equation in the fluid

Again in the context of the aforementioned assumptions, and with respect to the cross-section of the internally finned duct and the Cartesian coordinate system depicted in Fig. 1, in the thermally fully developed region, the energy equation in the fluid reduces to the following form [64,65]:

$$\rho c_p w \frac{\partial T}{\partial z} = \frac{\partial}{\partial x}\left(k_f \frac{\partial T}{\partial x}\right) + \frac{\partial}{\partial y}\left(k_f \frac{\partial T}{\partial y}\right) \tag{2}$$

In this equation, $T$ is the temperature, $c_p$ is the specific heat at constant pressure, and $k_f$ is the thermal conductivity of the fluid.

### 2.3. Energy equation in the fins

In any cross-section of the duct, a quasi one-dimensional formulation [62,63] is used to model heat conduction inside the fins, following the approach adopted by Baliga and Azrak [20] for investigating triangular plate-fin ducts. The conditions necessary for the validity of quasi one-dimensional fin theory [62,63] are assumed to be met in the demonstration problem. This assumption is made mainly for economy of computational effort in the illustration of the proposed optimization methodology: in problems where this assumption is invalid, a two-dimensional heat conduction equation must be solved in the fin [62,63], and the related computational effort would be much higher than that need for solving the quasi one-dimensional problem considered here.

In the context of the aforementioned assumptions, and with respect to the duct cross-section and the related nomenclature illustrated in Fig. 1, the energy equation in the each fin reduces to the following form:

$$\frac{d}{d\xi}\left(\delta_{fin} k_{fin} \frac{dT_{fin}}{d\xi}\right) = -2k_f \left(\frac{\partial T}{\partial \eta}\right)_{fluid,\eta=0} \tag{3}$$

In this equation, $T_{fin}$ is the quasi one-dimensional temperature inside the fin; $k_{fin}$ is the thermal conductivity of the fin material; $\xi$ is a coordinate along the centreline of the fin in the duct cross-section, with its origin at the fin base and increasing in the direction of its tip, as shown in Fig. 1; $\eta$ is the local coordinate normal to the fin surface at all points along it, with its origin at the fin surface and increasing in the direction of the fluid, as shown in Fig. 1; $\delta_{fin}$ is the local fin thickness at $\xi$; and $(\partial T/\partial \eta)_{fluid,\eta=0}$ is the local normal ($\eta$-direction) temperature gradient *in the fluid* at the surface of the fin.

### 2.4. Boundary conditions

#### 2.4.1. Fluid flow

In the fully-developed flow region, $u = v = 0$, and the boundary conditions on the $z$-direction component of the fluid velocity, $w$, are the following: along the duct wall and fin surfaces, the no-slip condition applies and $w = 0$; along symmetry surfaces, $\nabla_\perp w = 0$, where $\nabla_\perp w$ is the gradient of $w$ normal to the symmetry surface at the point under consideration.

#### 2.4.2. Thermal

At each point located on the interface between the fluid and a fin, the fin and fluid temperature are the same, as are the corresponding normal heat fluxes. Along symmetry surfaces, $\nabla_\perp T = 0$, where $\nabla_\perp T$ is the gradient of $T$ normal to the symmetry surface at the point under consideration. At the duct wall-fluid interface, the following two boundary conditions, which represent the extremes of the conditions that yield corresponding thermally fully-developed regimes [66], are considered:

**(H)**: Uniform rate of heat input per unit axial length ($q'_w$ = constant) and duct wall temperature, $T_w$, uniform *in the cross-section being considered*, but varying axially.
**(T)**: Uniform duct wall temperature axially *and* peripherally ($T_w$ = constant).

### 2.5. Dimensionless formulation

#### 2.5.1. z-Momentum equation

Following Shah and London [65], Patankar [60], and Kays and Crawford [64], the following dimensionless variables are introduced:

$$X = x/D_h; \quad Y = y/D_h; \quad W = w\mu/\{(-dP/dz)(D_h)^2\};$$
$$D_h = 4A_{c\text{-}s}/Peri_{wetted} \tag{4}$$

Here, $A_{c\text{-}s}$ is the cross-sectional area for fluid flow and $Peri_{wetted}$ is the wetted perimeter around this area (total length of the solid-fluid interface portion of $A_{c\text{-}s}$). Introducing these dimensionless variables in Eq. (1) and rearranging, the following dimensionless form of the $z$-momentum equation is obtained:

$$\frac{\partial^2 W}{\partial X^2} + \frac{\partial^2 W}{\partial Y^2} + 1 = 0 \tag{5}$$

The boundary conditions on $W$ are the following: $W = 0$ on the duct wall and the fin surfaces; and along symmetry surfaces, $\nabla_\perp W = 0$.

The only free dimensionless parameters in the fluid flow problem are those that characterize the cross-sectional geometry of the internally finned duct, which come into play when the boundary conditions are imposed. However, as the focus in this demonstration problem is on laminar flows, it is important to ensure that the value of the Reynolds number satisfies the following condition:

$$Re \triangleq \rho w_{av} D_h/\mu \le 2000 \tag{6}$$

The constant axial gradient of the reduced pressure in the fully developed region is expressed in dimensionless form as the Darcy friction factor, and the product of this friction factor and the Reynolds number is a constant for a given set of geometric parameters [64,65]:

$$f_{Darcy} \triangleq \{(-dP/dz)D_h\}/(\rho w_{av}^2/2);$$
$$f_{Darcy} Re = (2(-dP/dz)(D_h)^2)/(\mu w_{av}) = (2/W_{av}) \tag{7}$$

#### 2.5.2. Energy equations

The axial variations of the temperature for the two aforementioned thermal boundary conditions, (H) and (T), are different [60,62–64]. Thus, the dimensionless mathematical models for these two boundary conditions are formulated differently, as described in the following subsections.

*2.5.2.1. (H) Boundary condition.* For this boundary condition, in the thermally fully developed region, *all* temperatures (in the fluid, fin, and duct wall) rise linearly with $z$ [64–66]. Thus, with $T_b$ and $T_w$ denoting the fluid bulk and the duct wall temperatures, respectively, the following equation applies:

$$\frac{\partial T}{\partial z} = \frac{dT_b}{dz} = \frac{dT_w}{dz} = \text{constant} \tag{8}$$

Furthermore, an energy balance on a slice of the duct yields:

$$\rho w_{av} A_{c\text{-}s} c_p \frac{dT_b}{dz} = q'_w \tag{9}$$

At this stage, the following dimensionless temperature is introduced [60,64–66]:

$$\theta = (T_w - T)/(q'_w/k_f) \tag{10}$$

For the (H) boundary condition, $\theta$ is independent of the axial position along the duct (not a function of $z$) [60,64–66]. Thus, using $X$, $Y$, $W$, $\theta$, and $D_h$ in Eqs. (2) and (3), and rearranging, the dimensionless energy equations in the fluid and the fin can be obtained and cast in the following forms, respectively:

$$\frac{\partial^2\theta}{\partial X^2} + \frac{\partial^2\theta}{\partial Y^2} + 4\frac{D_h}{Peri_{wetted}}\frac{W}{W_{av}} = 0 \tag{11}$$

$$\frac{d}{d\Xi}\left(\Omega\frac{d\theta_{fin}}{d\Xi}\right) = -\left(\frac{\partial\theta}{\partial N}\right)_{fluid,N=0}; \quad \Omega = \frac{(\delta_{fin}/2)k_{fin}}{D_h k_f} \tag{12}$$

In Eq. (12), $\Xi = \xi/D_h$, $N = \eta/D_h$, and $\Omega$ is a dimensionless fin conductance based on its local half-thickness $(\delta_{fin}/2)$ at $\Xi$. On the duct wall, $T = T_w$, thus $\theta = 0$; and at symmetry surfaces, $\nabla_\perp\theta = 0$. At points located on the interface between a fin and the fluid, the values of $\theta$ in the fin and the fluid are the same. It should also be noted that for a given set of geometric parameters and $\Omega$, once the dimensionless velocity field $(W/W_{av})$ has been computed, the source term in Eq. (11) can be obtained, and Eqs. (11) and (12), along with the aforementioned boundary conditions, can be solved for the $\theta$ distribution.

With regard to processing of the results, the average Nusselt number for this boundary condition, $Nu_{av}^{(H)}$, is related to the dimensionless bulk temperature, $\theta_b$, by the following equation:

$$Nu_{av}^{(H)} = \frac{h_{av}D_h}{k_f} = \frac{\{(q'_w/Peri_{wetted})/(T_w - T_b)\}D_h}{k_f} = \frac{(D_h/Peri_{wetted})}{(T_w - T_b)/(q'_w/k_f)} = \frac{(D_h/Peri_{wetted})}{\theta_b} \tag{13}$$

*2.5.2.2. (T) Boundary condition.* For this boundary condition, the duct wall temperature, $T_w$, is specified and constant throughout, and a dimensionless axial coordinate, $z^*$, and dimensionless temperature, $\varphi$, are used [60,64–66]:

$$z^* = (z/D_h)/(RePr); \quad \varphi = (T_w - T)/(T_w - T_b); \quad Pr = \mu c_p/k_f \tag{14}$$

In this equation, $Pr$ denotes the Prandtl number.

In this case, in the thermally fully developed region, the magnitude of *all* temperature differences $(T_w - T)$, including $(T_w - T_b)$, decay exponentially with $z$ [60,64–66]; and the *local* heat transfer coefficient, $h = q''_w/(T_w - T_b)$, its peripherally averaged value in the cross-section of interest, $h_{av}$, and $\varphi$, *all* remain invariant with $z$ [60,64–66]. Thus,

$$(T_w - T_b) = A\exp(-\Lambda z^*); \quad \frac{d(T_w - T_b)}{dz^*} = -\Lambda(T_w - T_b);$$
$$\frac{1}{(T_w - T_b)}\frac{\partial T}{\partial z^*} = \Lambda\varphi \tag{15}$$

In this equation, $A$ and $\Lambda$ are constants. Using $X$, $Y$, $z^*$, $\varphi^* = \varphi/\Lambda$, and Eq. (15), the energy equations in the fluid and the fin, Eqs. (2) and (3), respectively, can be cast in the following dimensionless forms:

$$\frac{\partial^2\varphi^*}{\partial X^2} + \frac{\partial^2\varphi^*}{\partial Y^2} + \varphi^*\Lambda\frac{W}{W_{av}} = 0 \tag{16}$$

$$\frac{d}{d\Xi}\left(\Omega\frac{d\phi^*_{fin}}{d\Xi}\right) = -\left(\frac{\partial\phi^*}{\partial N}\right)_{fluid,N=0}; \quad \Omega = \frac{(\delta_{fin}/2)k_{fin}}{D_h k_f} \tag{17}$$

InIn Eq. (17), $\Xi = \xi/D_h$ and $N = \eta/D_h$; and $\Omega$ is a dimensionless fin conductance based on its local half-thickness $(\delta_{fin}/2)$ at $\Xi$. On the duct wall, $T = T_w$, thus $\varphi^* = 0$; and at symmetry surfaces, $\nabla_\perp\varphi^* = 0$. At points located on the interface between a fin and the fluid, the values of $\varphi^*$ in the fin and the fluid are the same. Furthermore, $\varphi_b = 1$, thus $\varphi^*_b = 1/\Lambda$. Therefore, for a given set of geometric parameters, $k_f$, and $k_{fin}$, once the dimensionless velocity field $(W/W_{av})$ has been computed, the $\varphi^*$ field and $\Lambda$ can be obtained using the following iterative procedure recommended by Patankar [60]: (1) guess an initial $\varphi^*$ field, calculate $\varphi^*_b$, and then obtain $\Lambda = 1/\varphi^*_b$; (2) using the calculated value of $\Lambda$ in Eq. (16), and the aforementioned boundary conditions, solve Eqs. (16) and (17) for a new distribution of $\varphi^*$; (3) calculate $\varphi^*_b$, and obtain a new value of $\Lambda = 1/\varphi^*_b$; and (4) return to Step (2), and repeat this procedure until convergence. Once the $\varphi^*$ field and $\Lambda$ have been calculated in this manner, the $\varphi$ field can be obtained using $\varphi = \Lambda\varphi^*$.

With regard to processing of the results, using the definition of $D_h$ in Eq. (4), the energy balance on a slice of the duct as expressed in Eq. (9), and the relations given in Eq. (15), the average Nusselt number for this case, $Nu_{av}^{(T)}$, can be related to $\Lambda$ by the following equation:

$$Nu_{av}^{(T)} = \frac{h_{av}D_h}{k_f} = \frac{\{(q'_w/Peri_{wetted})/(T_w - T_b)\}D_h}{k_f} = \frac{A_{c-s}}{Peri_{wetted}D_h}\Lambda = \frac{\Lambda}{4} \tag{18}$$

### 2.6. Numerical solution methods

In numerical solutions of the aforementioned mathematical models of steady, laminar, fully-developed flow and heat transfer phenomena in the demonstration problem, the calculation domain was limited to a representative portion of the duct cross-section, bounded by two adjacent symmetry surfaces, as shown schematically in Fig. 2. The $z$-momentum equation, Eq. (5), and the energy equations for the (H) and (T) thermal boundary conditions, Eqs. (11) and (16), respectively, are akin to equations that govern steady conduction-type problems [60]. These equations were solved using a control-volume finite element method (CVFEM) [56,57]. The quasi one-dimensional energy equations in the fin for the (H) and (T) boundary conditions, Eqs. (12) and (17), respectively, were solved using a finite volume method (FVM) [60]. Synopses of these numerical solution methods are provided in this section.

#### 2.6.1. Control-volume finite element method

The CVFEM used for the solution of the Eqs. (5), (11), and (16) was formulated using the following six steps: (1) discretization

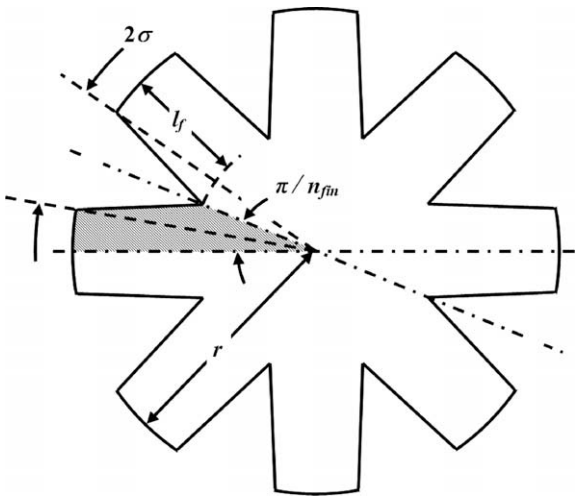


**Fig. 2.** Calculation domain, bounded by two adjacent symmetry planes with an angle of $\pi/n_{fin}$ between them, and related nomenclature.

of the portion of the calculation domain occupied by the fluid, first into three-node triangular elements and then into polygonal control volumes surrounding the nodes (these control volumes are created by joining the centroids of the triangular elements to the midpoints of the corresponding sides), as shown in Figs. 3(a) and (b); (2) integration of Eqs. (5), (11), and (16), in conjunction with the corresponding boundary conditions, over each of the polygonal control volumes to obtain integral momentum and energy conservation equations; (3) storage of the values of $W$, $\theta$, and $\varphi^*$ at the nodes of the finite element mesh, and linear interpolation of these nodal values in each triangular element; (4) in each three-node triangular element, storage of the values of the corresponding source terms at the centroid and assuming these values prevail over the element; (5) use of the aforementioned interpolation functions for the dependent variables and source terms to derive algebraic approximations to the aforementioned integral momentum and energy conservation equations; and (6) solution of these discretized equations using suitable iterative methods. Full details of this method are available in the works of Baliga and Patankar [56] and Baliga and Atabaki [57], so they are not repeated here.

*2.6.2. Finite volume method*

This method was used to solve the quasi one-dimensional heat conduction equations in the fin, Eqs. (12) and (17). The steps in its formulation are the following: (1) discretization of the fin into control volumes and associated nodes that match up with the adjacent portions of the polygonal control volumes and nodes of the aforementioned CVFEM, as illustrated schematically in Fig. 3 (b); (2) integration of Eqs. (12) and (17) over each of the control volumes surrounding the nodes to obtain integral energy conservation equations in the fin; (3) storage of $\theta$ and $\varphi^*$ at the nodes in the fin, and piecewise-linear interpolation of these variables over the grid lines between adjacent nodes; (4) storage of the fin conductance, $\Omega$, at the nodes in the fin, and use of piecewise-linear interpolation between adjacent nodes to calculate the values of $\Omega$ at the locations of the control-volume faces; (5) calculation and storage of $(\partial\varphi^*/\partial N)_{fluid,N=0}$ at the nodes in the fin, using solutions generated by the aforementioned CVFEM, and assuming that these values prevail over the corresponding portions of the control-volume boundary that fall along the fin-fluid interface; (6) use of the aforementioned interpolation functions for $\theta$, $\varphi^*$, $\Omega$, and $(\partial\varphi^*/\partial N)_{fluid,N=0}$ to derive algebraic approximations to the integral energy conservation equations in the fin; and (6) solution of these discretized equations using the tri-diagonal matrix algorithm [60].

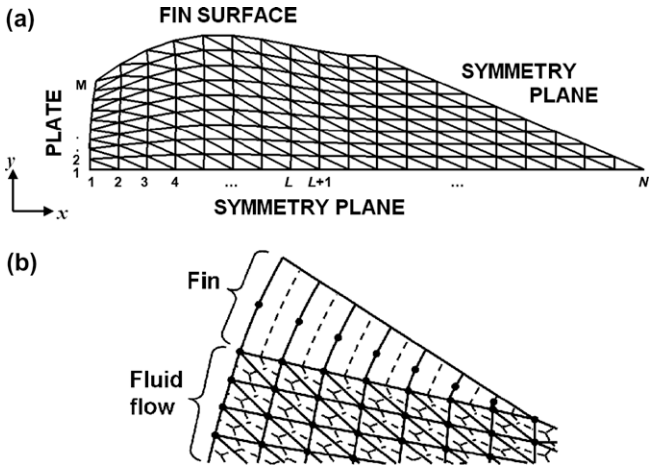


**Fig. 3.** (a) Three-node triangular elements used in the discretization of the fluid flow region and related nomenclature and (b) FVM grid in the fin and a portion of the CVFEM mesh (with the three-node triangular elements and the associated polygonal control volumes) in the adjacent fluid flow region.

## 3. Representation of the fin surface using non-uniform rational B-splines (NURBS)

In order to modify or adjust the shape of the fins in the overall optimization methodology, their surface (which is the interface between the fin and the fluid regions of the ducts) must first be described mathematically. As was discussed earlier, in the numerical solution of the demonstration problem, the calculation domain was limited to the representative portion of a cross-section of the duct shown in Fig. 2: in this calculation domain, the fin surface is a curve. A single polynomial representation of this curve is often inefficient or unsuitable for interactive shape design [55]. A common practice for overcoming this difficulty is to split the curve into multiple *piecewise polynomials* or *rational* curves, and set rules that ensure continuity and smoothness at the locations where these curves meet. Such curves are called *splines*. On a spline, the locations in space where the piecewise curves meet are called the control points: they can be conveniently expressed in vector form as $\mathbf{P} = \{\mathbf{P}_1, \mathbf{P}_2, \ldots, \mathbf{P}_i, \ldots, \mathbf{P}_n\}$. A polygon whose summits are the control points is called the *control polygon*.

A spline in which each control point is associated with a *basis function* is called a B-spline. These basis functions define the portion of the spline that is affected by each control point, and allow *local* modification of the shape of a curve (so only the portion of the curve close to the control point is affected). Thus, on a B-spline, each control point affects a user-defined portion of the curve and they all have the same weight.

A generalised version of a B-spline is the so-called non-uniform rational B-spline (NURBS), which is defined by its order, a set of weighted control points, and a knot vector. The *order* of a NURBS curve defines the number of nearby control points that influence any given control point: the curve is represented by polynomial basis functions of degree one *less* than its order, and the number of control points must be greater than or equal to the order. The knot vector is a sequence of parameter values that determine where and how the control points affect the NURBS curve along its length, and is represented as follows: $U = \{u_1, u_2, \ldots, u_i, \ldots, u_n\}$ $0 \leqslant u \leqslant 1$. For applications with a smooth continuous curve, a uniform knot vector, in which $u_{i+1} - u_i$ = constant, $\forall i$, is adequate, since by controlling the number and position of the control points and their weights, the NURBS can be used to fit almost any shape [55]. This type of knot vector is implemented for approximating the fin shape in this work.

A $p$th degree NURBS curve can be expressed as follows:

$$\mathbf{C}(u) = \sum_{i=0}^{n} R_{i,p}(u)\mathbf{P}_i; \quad R_{i,p}(u) = (N_{i,p}(u)w_i) \Big/ \left(\sum_{j=0}^{n} N_{j,p}(u)w_j\right); \quad 0 \leq u \leq 1 \tag{19}$$

where $\{R_{i,p}(u)\}$ are *rational basis functions* of the NURBS curve, $\{\mathbf{P}_i\}$ are the control points (forming a *control polygon*), and $\{w_i\}$ are the weights associated with the control points. $\{N_{i,p}(u)\}$ are the $p$th degree B-spline basis functions associated with the control points and defined on the following open uniform knot vector:

$$\mathbf{U} = \{\underbrace{a, \ldots, a}_{p+1}, u_{p+1}, \ldots, u_{n-p-1}, \underbrace{b, \ldots, b}_{p+1}\} \tag{20}$$

where $a = 0$, $b = 1$ and $w_i > 0$ for all $i$. Repeating the knot situated at both ends of the vector $p + 1$ times ensures that the outer extreme points of the curve fall on the control points tangentially at the two end portions of the control polygon. In this work, the following computationally convenient recurrence formula was used to prescribe the basis functions:

$$N_{i,0}(u) = \begin{cases} 0 & \text{if } u_i \leq u \leq u_{i+1} \\ 1 & \text{otherwise} \end{cases}; \quad N_{i,p}(u) = \frac{u - u_i}{u_{i+p} - u_i} N_{i,p-1}(u) + \frac{u_{i+p+1} - u}{u_{i+p+1} - u_{i+1}} N_{i+1,p-1}(u) \tag{21}$$

In practice, the most commonly used NURBS curves are of fourth order (cubic degree), as they are sufficient to approximate rather complex shapes quite well [55]: these curves were also used in this work. With respect to the demonstration problem, the approximation of a representative fin shape in the calculation domain using an open uniform rational fourth-order B-spline curve with six control points is shown in Fig. 4. The position of each control point $\mathbf{P}_i$ is defined by its radial distance *from* the wall of the circular duct, $r_i$, and its elevation above the fin central symmetry surface, $h_i$. The first control point, $\mathbf{P}_1$, is situated directly on the duct wall, so $r_1 = 0$ and its height, $h_1$, sets the fin half-width at its base. The last control point, $\mathbf{P}_n$, is situated directly on the fin central symmetry surface, so that its height, $h_n$, is 0, and its radial position from the duct wall, $r_n$, is equal to the length of the fin, $l_f$. In the computer simulations that were undertaken in this work, the radial positions from the duct wall of the remaining interior control points, $r_i$, were distributed uniformly along the fin length, and the weights, $w_i$, of the control points were all set equal to one. Thus, the following parameters were modified to change the shape of the fin: the number of control points, $n$; the height of the first $(n-1)$ control points, $h_i$; and the radial position from the wall of the $n$th control point, $r_n = l_f$. These parameters were adjusted in the search for an optimal fin shape, as discussed in the following section.

## 4. Formulation of the optimization problem

The problem of interest is a static, non-linear, multivariable optimization problem, subject to an equality constraint and involving the maximization of an objective function that is specific to each of the two boundary conditions, (H) and (T) [24]. The mathematical formulation of this optimization problem can be expressed in the following general form:

$$\text{Find } \mathbf{X} = \begin{Bmatrix} x_1 \\ x_2 \\ \vdots \\ x_n \end{Bmatrix} \text{ which maximizes } f(\mathbf{X}), \text{ subject to } g(\mathbf{X}) = \text{constant} \tag{22}$$

In this equation, $\mathbf{X}$ is an $n$-dimensional *design vector* containing the design variables, $x_i$; $f(\mathbf{X})$ is the *objective function*; and $g(\mathbf{X})$ is the *equality constraint function*. The $n$-dimensional space, in which each coordinate axis represents a design variable, is called the *design space*, and each point $\mathbf{X}$ in it is called a *design point*. The design variables, the objective functions, and the equality constraint considered in this study are presented concisely in this section.

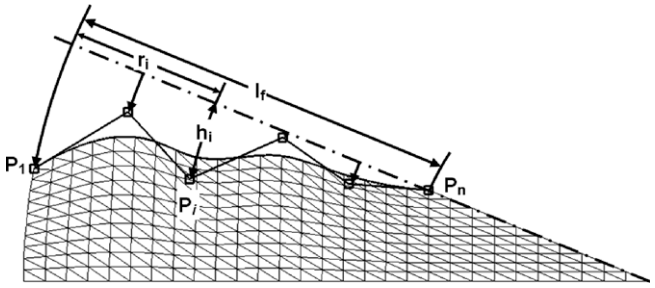


**Fig. 4.** Approximation of the surface of a representative fin in the calculation domain using an open uniform rational B-spline curve with six control points (indicated by the symbol □ and denoted as $\mathbf{P}_i$), the three-node triangular elements used in the CVFEM mesh in the fluid flow region, and related nomenclature.

### 4.1. Design variables

With reference to Fig. 4 and the NURBS approximation of the fin surface discussed in the last section, the chosen design variables were the heights of the first $(n-1)$ control points above the fin symmetry surface, and the length of the fin for the $n$th control point ($l_f = r_n$):

$$\mathbf{X} = \begin{Bmatrix} x_1 \\ x_2 \\ \vdots \\ x_{n-1} \\ x_n \end{Bmatrix} = \begin{Bmatrix} h_1 \\ h_2 \\ \vdots \\ h_{n-1} \\ l_f \end{Bmatrix} \tag{23}$$

In order to avoid any possible dimensional inhomogeneity and large differences in the magnitudes of the design variables, and related difficulties [23,24], they were scaled and cast in dimensionless forms with respect to their minimum and maximum values, as follows:

$$x_i^* = (x_i - x_{i,\min})/(x_{i,\max} - x_{i,\min}) \tag{24}$$

The minimum and maximum values, $x_{i,\min}$ and $x_{i,\max}$, respectively, for each variable depend on the particular optimization problem being solved, and they are set by reference to either physical limits (for example, a length can not be lower than 0), structural integrity requirements (for example, a minimum thickness of the fin), or geometric limits (for example, a limit on the maximum thickness of the fin). Each dimensionless design variable, $x_i^*$, must lie between 0 and 1. If the value of any $x_i^*$ falls outside this allowed range during any stage of the iterative optimization process, special care must be taken to ensure that the size and direction of the next step in this process leads this value back inside the allowed range (this special treatment is elaborated further in Section 4.4.3).

### 4.2. Objective functions

The criterion with respect to which the design is optimized is called the *objective function*. It is a function of the design variables and takes on a finite value for each point in the design space. As was stated earlier, two different thermal boundary conditions, (H) and (T), were considered in this work: thus, two different objective functions were proposed, and the corresponding two separate optimization problems were solved. The goal in each of these two optimization problems was to determine the shape of the fins that *maximize* the chosen objective function, subject to imposed constraints which are defined in the next subsection.

#### 4.2.1. (H) Boundary condition

For this thermal boundary condition, $q'_w$ is constant everywhere and $T_w$ is uniform in any cross-section but varies axially. With regard to the optimal thermal performance, it is proposed that in any given cross-section in the fully developed region, the specified constant value of $q'_w$ should be achieved with the minimum value of $(T_w - T_b)$: in dimensionless terms, this requirement is equivalent to the maximization of $1/\theta_b = (q'_w/k_f)/(T_w - T_b)$. Thus, using the average Nusselt number for this case, $Nu_{av}^{(H)}$, as defined in Eq. (13), the objective function for this boundary condition can be defined as follows:

$$f^{(\mathrm{H})}(\mathbf{X}) = Nu_{av}^{(H)}(Peri_{wetted}/D_h) \tag{25}$$

#### 4.2.2. (T) Boundary condition

For this thermal boundary condition, $T_w$ is constant everywhere, peripherally and axially. In this case, with regard to the optimal thermal performance, it is proposed that in any given cross-section

in the fully developed region, the maximum value of $q'_w$ should be achieved with the minimum value of $(T_w - T_b)$: in dimensionless terms, this requirement is equivalent to the maximization of $(q'_w/k_f)/(T_w - T_b)$. Thus, using the average Nusselt number for this case, $Nu_{av}^{(T)}$, as defined in Eq. (18), the objective function for this boundary condition can be defined as follows:

$$f^{(T)}(\mathbf{X}) = Nu_{av}^{(T)}(Peri_{wetted}/D_h) \tag{26}$$

### 4.3. Constraint function

In most practical problems, the design variables have to satisfy certain specified functional and/or other requirements. Such requirements are called *design constraints*. In this demonstration problem, the chosen goal is the following: for a given combination of internally finned duct, fin material, and fluid, identify the fin shape that optimizes the thermal performance (maximizes the above-mentioned objective functions) in the fully developed region for a specified constant pumping power needed to overcome the viscous losses per unit length of the duct. This pumping power per unit length for the laminar fully-developed flows of interest can be expressed in terms of the axial gradient of the reduced pressure as follows:

$$pp = (-dP/dz)w_{av}A_{c\text{-}s} \tag{27}$$

where $A_{c\text{-}s}$ is the total cross-sectional area for the fluid flow in the internally finned duct. The requirement in the demonstration problem is that this pumping power per unit length must remain constant (fixed) at a specified target value, $pp_{target}$, for the optimal solution to be acceptable. In this context, the constraint function, $g(\mathbf{X})$, is based on the square of the difference between $pp$ and $pp_{target}$, normalized with respect to $pp_{target}$, and the constraint requirement is to drive this function down to zero:

$$\begin{aligned} g(\mathbf{X}) &= \{(pp - pp_{target})/pp_{target}\}^2 \\ &= \{((-dP/dz)w_{av}A_{c\text{-}s} - pp_{target})/pp_{target}\}^2 = 0 \end{aligned} \tag{28}$$

With this definition of $g(\mathbf{X})$, the magnitude of its gradient decreases monotonically as the optimization algorithm gets closer to the desired value of $\mathbf{X}$. This feature allows the use of a search method with the step size proportional to this gradient, so that it decreases monotonically, in an adaptive manner, until it becomes null when the desired value of $\mathbf{X}$ is reached. Eq. (28) defines a hyper-plane in the $n$-dimensional space spanned by the design variables. The optimal solution must lie on this hyper-plane in order to satisfy the constraint requirement.

### 4.4. Optimization algorithm

The proposed optimization algorithm is a variation of Rosen's gradient projection method [24], which, in turn, is based on the more general class of gradient, or steepest descent, methods [23,24,31]. The method is divided into two main parts: satisfaction of the constraint function; and optimization of the objective function. A distinction is made between these two parts because the corresponding search direction and step size are different. These two parts of the optimization algorithm are presented in Sections 4.4.1 and 4.4.2. Then, a special treatment that is used to effect corrections of the optimization path when the design point falls outside the allowed design space is presented in Section 4.4.3. Finally, a note on the optimization parameters and a synopsis of the overall algorithm are presented in Section 4.4.4.

#### 4.4.1. Satisfaction of the constraint requirement

The initial point, $\mathbf{X}_{ini}$, at the start of the iterative optimization procedure, can be anywhere in the design space and, in general, will not be located on the constraint hyper-plane. In the proposed optimization algorithm, the design point, $\mathbf{X}$, is first moved on to the constraint hyper-plane; following that, the search for the optimal solution is carried out, while ensuring that $\mathbf{X}$ stays on this constraint hyper-plane.

The step-by-step process of moving the design point from its initial location to the constraint hyper-plane is implemented as follows:

$$\mathbf{X}_{m+1} = \mathbf{X}_m + \lambda_m \mathbf{S}_m \tag{29}$$

where $\mathbf{X}_m$ is the current design point, $\mathbf{X}_{m+1}$ is the next design point, $\mathbf{S}_m$ is the normalized search-direction vector, and $\lambda_m$ is the associated step size. The gradient of the constraint function and its norm are defined as follows:

$$\nabla g(\mathbf{X}_m) = \left[\frac{\partial g}{\partial x_1}, \ldots, \frac{\partial g}{\partial x_j}, \ldots, \frac{\partial g}{\partial x_n}\right]_m; \quad \|\nabla g(\mathbf{X}_m)\| = \left[\left\{\sum_{j=1}^{n}\left(\frac{\partial g}{\partial x_j}\right)^2\right\}^{1/2}\right]_m \tag{30}$$

The gradient vector points in the direction of steepest *ascent*, thus its negative value is used to define the normalized search-direction vector in this part of the optimization algorithm, so as to ensure the steepest *descent* towards the constraint requirement of $g(\mathbf{X}_m) = 0$:

$$\mathbf{S}_m = -\nabla g(\mathbf{X}_m)/\|\nabla g(\mathbf{X}_m)\| \tag{31}$$

The step size, $\lambda_m$, is selected as follows:

$$\lambda_m = \lambda_{constraint}\|\nabla g(\mathbf{X}_m)\|/\|\nabla g(\mathbf{X}_{ini})\| \tag{32}$$

where $\lambda_{constraint}$ is a specified reference step size. This approach makes it possible to start with a chosen initial step size, $\lambda_{constraint.ini}$, and ensure that each successive step size, which is proportional to $\|\nabla g(\mathbf{X}_m)\|$, decreases continuously and monotonically as the constraint hyper-plane is approached. This gradient-based search algorithm moves the design point, $\mathbf{X}_m$, from its initial position step-by-step towards the constraint hyper-plane until the following criterion is satisfied:

$$g(\mathbf{X}_m) \le \varepsilon_{constraint} \tag{33}$$

Once this criterion is met, the design point is considered to have satisfied the constraint requirement, and the search is then focused on meeting the optimization criterion (maximization of the objective function) while keeping the design point on the constraint hyper-plane.

#### 4.4.2. Maximization of the objective function

In order to obtain a search direction that allows an increase in the value of the objective function while at the same time satisfying the constraint requirement, $\nabla f(\mathbf{X}_m)$ is first projected onto the constraint hyper-plane, which is normal to $\nabla g(\mathbf{X}_m)$. This projected vector is denoted as $\nabla f_{proj}(\mathbf{X}_m)$: it is graphically presented in Fig. 5 for a three-dimensional design space ($n = 3$). A step-by-step process akin to that expressed in Eq. (29) is then used to move the design point along the constraint hyper-plane, with the normalized search-direction vector, $\mathbf{S}_m$, and step size, $\lambda_m$, defined as follows:

$$\mathbf{S}_m = \nabla f_{proj}(\mathbf{X}_m)/\|\nabla f_{proj}(\mathbf{X}_m)\|; \quad \lambda_m = \lambda_{obj}\|\nabla f_{proj}(\mathbf{X}_m)\|/\|\nabla f_{proj}(\mathbf{X}_{ini})\| \tag{34}$$

The resulting search direction satisfies the constraint function (that is, the design point is located within the specified tolerance, $\varepsilon_{constraint}$, of the constraint hyper-plane), and it also moves the objective function towards its maximum value at the next step or design point. Fig. 6 shows the behaviour of a sample optimization path in a two-dimensional design space ($n = 2$): first, the design point is moved towards the constraint hyper-plane; and once the constraint requirement is achieved to within the specified tolerance, the afore-

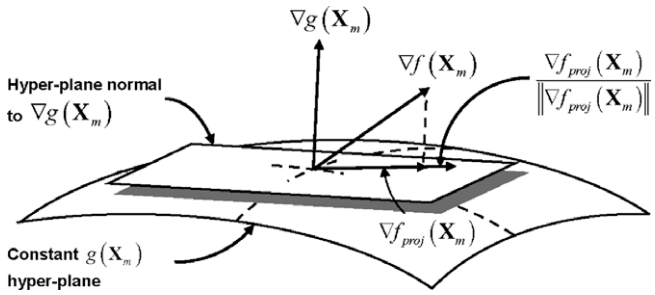


**Fig. 5.** Projection of $\nabla f(\mathbf{X}_m)$ onto the hyper-plane normal to $\nabla g(\mathbf{X}_m)$ for a three-dimensional design space ($n = 3$).

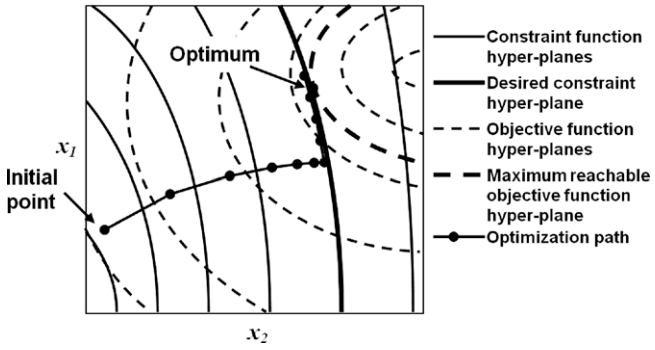


**Fig. 6.** Sample optimization path in a two-dimensional design space ($n = 2$).

mentioned procedure is used to move the design point towards its optimal location (which maximizes the objective function) along the constraint hyper-plane.

*4.4.3. Special treatment at the boundary of the design space*

The optimization path, such as that shown in Fig. 6 for $n = 2$, can sometimes lead outside the allowed design space: this situation could be encountered, for example, when the constraint hyper-plane is close to the limits of the dimensionless design variables, $x_i = 0$ or 1, or if the initial design point is located close to these limits. If any particular step along the optimization path takes the design point outside the allowed design space, then the direction of the optimization path must be corrected so that this design point is moved back within the allowed design space. The special treatment that is implemented to achieve such a correction depends on the current state of the optimization procedure: that is, whether the optimization path is in its first phase, and moving the design point towards the constraint hyper-plane, or second phase, and moving the design point along the constraint hyper-plane towards the optimum solution (see the example given in Fig. 6 for $n = 2$).

If the optimization path is moving the design point towards the constraint hyper-plane, the algorithm is navigating freely in the design space: that is, it is not restricted to a constraint hyper-plane. Thus, if a design-space boundary is encountered or crossed, the corresponding step size, $\lambda_m$, is maintained, but the search-direction vector, $\mathbf{S}_m$, is replaced by its projection onto the limiting hyper-plane being crossed ($x_i = 0$ or 1).

If the optimization path is moving the design point along the constraint hyper-plane towards the optimum solution, the corresponding step size, $\lambda_m$, is again maintained, and the search-direction vector, $\mathbf{S}_m$, is corrected. However, now, the corrected search-direction vector must not only be tangential to the limiting hyper-plane being crossed, but it must also lie on the constraint hyper-plane. This requirement is met using the following treatment: first, the *components* of $\mathbf{S}_m$ and $\nabla g(\mathbf{X}_m)$ *normal* to the limiting hyper-plane being crossed are set to zero, making the remaining portions of these two vectors tangential to the limiting hyper-plane; then, the modified *tangential* portion of $\mathbf{S}_m$ is projected onto the hyper-plane that is normal to the aforementioned *tangential* portion of $\nabla g(\mathbf{X}_m)$ .

*4.4.4. Note on parameters and synopsis of algorithm*

The parameters (step sizes and tolerances) involved in the proposed optimization algorithm were assigned the following values in the solution of the demonstration problem:

$$\lambda_{constraint,ini} = 0.1; \quad \lambda_{obj,ini} = 0.5\lambda_{constraint,ini};$$
$$\varepsilon_{constraint,ini} = 0.02; \quad \varepsilon_{final} = 10^{-5} \tag{35}$$

Starting with the initial values given in this equation, the tolerance, $\varepsilon_{constraint}$, and the reference step sizes, $\lambda_{constraint}$ and $\lambda_{obj}$, are either adjusted or kept unchanged in accordance with the following procedure: at any step, $m$, in the second phase of the optimization path (when the focus is on moving the design point along the constraint hyper-plane towards the optimum solution), if the maximum value of the objective function, $f(\mathbf{X})$, is overshot, that is $f(\mathbf{X}_m) < f(\mathbf{X}_{m-1})$, then the inner product of the search-direction vectors at the current and the previous steps, $\mathbf{S}_m \bullet \mathbf{S}_{m-1}$, is monitored; if this product is negative, $\mathbf{S}_m \bullet \mathbf{S}_{m-1} < 0$, for the following four consecutive steps ($m$, $m+1$, $m+2$, $m+3$), then $\varepsilon_{constraint}$ is reduced by a factor of five, and $\lambda_{constraint}$ and $\lambda_{obj}$ are reduced by a factor of three; and if the aforementioned condition is not met, $\varepsilon_{constraint}$, $\lambda_{constraint}$, and $\lambda_{obj}$ are left unchanged. These adjustments cause the search to be done with progressively smaller step sizes in the region of the design space that is expected to contain the optimal solution, and also move the search path progressively closer to the constraint hyper-plane. The reductions of the tolerance and step sizes are continued in this manner until the overall convergence criterion, namely, $\varepsilon_{constraint} \leqslant \varepsilon_{final}$, is satisfied. This adjustment procedure and the aforementioned reduction factors for $\varepsilon_{constraint}$, $\lambda_{constraint}$, and $\lambda_{obj}$ were chosen on basis of numerous preliminary computational trials, which showed that they allowed the optimal solution to be achieved in a relatively efficient manner.

The overall optimization algorithm can be summarized as follows:

1. Start with an initial design point, $\mathbf{X}_0$ (for example, the particular baseline case of the demonstration problem that is being optimized); assign initial values for $\varepsilon_{constraint}$, $\lambda_{constraint}$, and $\lambda_{obj}$; set $\mathbf{S}_1 = 1$; set the overall iteration or step counter to $m = 1$ (the starting iteration number is $m = 0$); and calculate $\mathbf{X}_1$ using Eq. (29).
2. Check if $g(\mathbf{X}_m) \leqslant \varepsilon_{constraint}$: if no, go to step 3; if yes, the constraint requirement is satisfied and the search for the optimal solution can be initiated, so go to step 4.
3. Using numerical differentiation of the CVFEM and FVM solutions of the direct problem (see descriptions of the mathematical models and numerical solution methods in Section 2) at the design point $\mathbf{X}_{m-1}$ and a series of $n$ different design points $\mathbf{X}_j = [(\{x_i\}_j = \{x_i\}_{m-1} + \lambda_{m-1}(s_i)_{m-1}\delta_{ij};\ i = 1, 2, \ldots, n)\ j = 1, 2, \ldots, n]$, where $\delta_{ij}$ is the Kronecker delta function, calculate each component of the gradient of the constraint function, $\nabla g(\mathbf{X}_m)$; then calculate $\mathbf{S}_m$ and $\lambda_m$ using the procedures described in Section 4.4.1; augment the step counter by one; calculate the new design point $\mathbf{X}_{m+1}$ using Eq. (29); use the special treatment presented in Section 4.4.3, if needed, to ensure that $\mathbf{X}_{m+1}$ lies within the allowed design space; and then return to Step 2.
4. Using numerical differentiation of the CVFEM and FVM solutions of the direct problem at the design point $\mathbf{X}_{m-1}$ and a series of $n$ different design points $\mathbf{X}_j = [(\{x_i\}_j = \{x_i\}_{m-1} + \lambda_{m-1}(s_i)_{m-1}\delta_{ij};\ i = 1, 2, \ldots, n)\ j = 1, 2, \ldots, n]$, where $\delta_{ij}$ is the Kronecker delta

function, calculate each component of the gradient of the objective function, $\nabla f(\mathbf{X}_m)$; then calculate $\nabla f_{proj}(\mathbf{X}_m)$, $\mathbf{S}_m$, and $\lambda_m$ using the procedures described in Section 4.4.2; calculate the new design point $\mathbf{X}_{m+1}$ using Eq. (29); use the special treatment presented in Section 4.4.3, if needed, to ensure that $\mathbf{X}_{m+1}$ lies within the allowed design space; and augment the step counter by one.

5. Adjust $\varepsilon_{constraint}$, $\lambda_{constraint}$, and $\lambda_{obj}$ using the procedure described at the start of this subsection.
6. Check if $\varepsilon_{const} \leqslant \varepsilon_{final}$: if no, return to Step 2; if yes, the optimum solution has been has been reached, so calculate any needed additional results, store all desired results, and then terminate the optimization procedure.

This gradient-based optimization methodology does not guarantee the absolute optimal solution, but it yields significant improvements in thermal performance of internally finned ducts. Sample results obtained for the aforementioned demonstration problem are presented and discussed in the next section.

## 5. Results and discussion

As was mentioned earlier, the demonstration problem used in this work involves steady, fully-developed, laminar forced convection in straight ducts (of circular cross-section) with non-twisted, continuous, longitudinal fins. Air ($k_f = k_{air} = 0.028$ W/m °C) is the working fluid, and the fin materials explored are stainless steel ($k_{fin} = k_{s.s.} = 15.1$ W/m °C), aluminium ($k_{fin} = k_{Al} = 237$ W/m °C), and copper ($k_{fin} = k_{Cu} = 401$ W/m °C). A schematic illustration of a cross-section of these ducts and the related notation used in this work are shown in Fig. 1. The calculation domain and the related nomenclature are presented in Fig. 2.

### 5.1. Cases considered

The proposed optimization methodology was applied to two different *baseline* cases of the demonstration problem, denoted as Cases 1 and 2, each with fins of triangular cross-section (starting fin shape before application of the optimization methodology). The performance yielded by the optimized fin shapes for each of these cases was compared to that of the corresponding baseline. For the *baseline* Case 1, the parameters were set to the following values: dimensionless length of the fins $l^* = l_f/r = 0.8$; the number of fins $n_{fin} = 8$; and the angle of each fin at its base $2\sigma = 6^\circ = \pi/30$ radians. For the *baseline* Case 2, the aforementioned parameters were set equal to the following values: $l^* = l_f/r = 0.6$, $n_{fin} = 16$, and $2\sigma = 3^\circ = \pi/60$. For each of these *baseline* cases, the target pumping power per unit length, $pp_{target}$, was determined with the duct radius set equal to $r = 6.35$ mm and a reduced pressure drop per unit length ($-dP/dz$) that yielded a Reynolds number of $Re = 100$. Cross-sections of these *baseline* internally finned ducts (with spatial dimensions normalized with respect to the duct radius, $r$) and the corresponding contours of dimensionless axial velocity ($W$) are presented in Fig. 7(a) and (b), respectively.

In both of the aforementioned cases, the following minimum and maximum values of the design variables relative to the radius, $r$, of the duct were used: $0.01 \leqslant (h_i/r) \leqslant [(\pi/n_{fin})\{1-(n-i)/(n-1)\}]$; and $0.2 \leqslant l^* \leqslant 0.9$. The minimum value of $(h_i/r)$ was chosen to ensure that for each fin, the local thickness did not take on values that made it too delicate, from either the mechanical strength or manufacturing points of view; and its maximum value was set so as to ensure that for each fin, the local thickness did not exceed that of a triangular fin with the same length as the optimal fin and a base thickness of $(2\pi r/n_{fin})$, the maximum geometrical value possible.

The improvement provided by an optimized duct over that of its baseline case for the same pumping power per unit length was quantified by calculating the following thermal performance enhancement indices, which are the ratios of the corresponding objective functions:

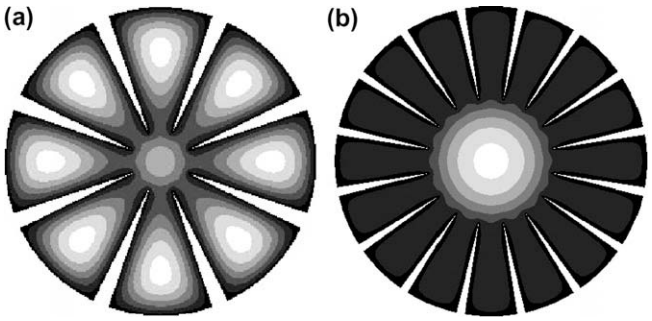


**Fig. 7.** Representative cross-section (with spatial dimensions normalized with respect to the duct radius, $r$) and fully-developed axial velocity contours in the baseline cases of the demonstration problem: (a) Case 1 and (b) Case 2.

$$\eta^{(H)} = \left[\left(f^{(H)}(\mathbf{X})\right)_{Optimized\ duct} / \left(f^{(H)}(\mathbf{X})\right)_{Baseline\ case}\right]$$
$$\eta^{(T)} = \left[\left(f^{(T)}(\mathbf{X})\right)_{Optimized\ duct} / \left(f^{(T)}(\mathbf{X})\right)_{Baseline\ case}\right] \quad (36)$$

### 5.2. Discretization of the fluid flow and fin regions

The fluid flow and fin regions of the calculation domain were discretized using CVFEM and FVM grids, respectively, akin to those shown in Fig. 3(a) and (b). The total number of nodes along the bottom symmetry plane, $L + N$, was specified. Next, the value of $L$ was obtained using the following equation:

$$L = \text{Closest integer roundoff of } [(L+N)(l_f/r)] \quad (37)$$

$N$ was then set equal to $(L + N) - L$. The portion of the calculation domain beyond $L + 1$ in the $x$ direction was discretized into triangular elements, each with the longest side oriented in the top-left-to-bottom-right direction, matching the top symmetry plane; and in this portion of the calculation domain, the numbers of nodes in the $x$ and the $y$ directions were the same and the node spacing was uniform. For the remaining portion of the calculation domain, once the positions of the control points were set (in each step of the optimization procedure) and the NURBS curve was computed, the grid points (nodes) along the fin surface were distributed uniformly on the NURBS curve. Then, the nodes on the duct wall were also distributed equidistantly between the first control point and the bottom symmetry plane. The positions of the remaining interior nodes were interpolated linearly between the surrounding bounding nodes, and then the horizontal position of each of these nodes set to averages of those of the four surrounding nodes: the resulting grid patterns were akin to that shown in Fig. 3(a) and (b).

Numerous preliminary investigations were carried out using ducts with internal fins of fixed triangular cross-section (akin to the aforementioned two *baseline* cases of this demonstration problem) and successively finer computational grids. The results of these preliminary investigations were then used in an extrapolation scheme, akin to that proposed by Richardson, to obtain essentially grid-independent solutions. These tests showed that grids with $(L + N) = 50$ give results that are within 0.05% of the aforementioned essentially grid-independent solutions. The final computations were all carried out with $(L + N) = 50$.

### 5.3. Effect of the number of control points

The effect of the number of control points (the design variables) on the shape of the optimized fin was investigated for the Case 1 baseline problem with the (H) thermal boundary condition and

the number of fins fixed at $n_{fin} = 8$. The proposed optimization methodology was applied to this problem with the five different values of the number of control points: $n = 4$, 6, 9, 12, and 15. The resulting optimized fin shapes are presented in Fig. 8(a)–(e): the continuous curve on the left side of each of these figures is a part of the perimeter of the circular cross-section of the duct; the long-and-short dashed lines represent radial symmetry surfaces; the control-point locations are indicated by the square symbols (□); the piecewise-straight lines joining these symbols constitute the control polygons; and the fin shapes are indicated by the solid curves along the top of each figure, immediately adjacent to the corresponding control polygons. With $n = 4$ and 6, the optimized fin shape has a bulge in its central region; and with $n = 9$, 12, and 15, the optimized fin shape has two bulges along its length, and its base width is larger than that of the baseline triangular fin. The optimized fin shapes obtained with $n = 12$ and 15 are very similar; there is only a slight difference in the widths of the fin base, which for $n = 15$ is slightly larger than that for $n = 12$. Based on these results, it was concluded that $n = 12$ is adequate for demonstrating the capabilities of the proposed optimization methodology.

### 5.4. Optimized internally finned ducts

The proposed optimization methodology was applied to the aforementioned two baseline problems, Cases 1 and 2, with the number of control points (design variables) fixed at $n = 12$ in each case. For Case 1 (the baseline case with eight internal fins of triangular cross-section), the fin shape was optimized for the following seven different values of the number of fins: $n_{fin} = 5$, 6, 7, 8, 9, 10, and 11. For Case 2 (the baseline case with 16 internal fins of triangular cross-section), the fin shape was optimized for the following seven different values of the number of fins: $n_{fin} = 7$, 8, 9, 10, 12, 14, and 16. The performance improvement indices for Case 1 are summarized in Table 1 for both the (H) and (T) boundary conditions, and the corresponding normalized fin shapes and contours of dimensionless axial velocity ($W$) are presented graphically in Fig. 9(a) and (b), respectively. For Case 2, these results are summarized in Table 2 and presented graphically in Fig. 10(a) and (b).

The quantitative results presented in Tables 1 and 2 show that at constant pumping power per unit length, the following increases in thermal performance of the optimized ducts relative to that of the corresponding baseline cases are obtained: for Case 1 and the (H) thermal boundary condition, $n_{fin} = 6$ yields $\eta^{(H)}$ values of 1.2547, 1.3206, and 1.2221 for the stainless steel, aluminium, and copper fins, respectively; for Case 1 and the (T) thermal boundary condition, $n_{fin} = 7$ yields $\eta^{(T)}$ values of 1.2192, 1.1532, and 1.1784 for the stainless steel, aluminium, and copper fins, respectively; for Case 2 and the (H) thermal boundary condition, $n_{fin} = 8$ yields $\eta^{(H)}$ values of 7.6800, 7.5813, and 7.6325 for the stainless steel, aluminium, and copper fins, respectively; and for Case 2 and the (T) thermal boundary condition, $n_{fin} = 9$ yields $\eta^{(T)}$ values of 10.681, 10.496, and 10.614 for the stainless steel, aluminium, and copper fins, respectively. For Case 1, the fluid flow in the *baseline* problem is already fairly well distributed in the regions between the fins, as shown by the dimensionless axial velocity contours in Fig. 7(a): thus, the improvements in thermal performance yielded by the optimized ducts are relatively modest for this case. On the other hand, for Case 2, the fluid flow in the *baseline* problem is rather poorly distributed, with most of it in the central region of the duct and only relatively low-velocity flow in the regions between the fins, as shown by the dimensionless axial velocity contours in Fig. 7(b): thus, the optimized ducts provide dramatic improvements in the relative thermal performance for this case.

**Table 1**
Results provided by the optimization methodology for Case 1.

| $n_{fin}$ | Stainless steel | | Aluminium | | Copper | |
|---|---|---|---|---|---|---|
| | $\eta^{(H)}$ | $\eta^{(T)}$ | $\eta^{(H)}$ | $\eta^{(T)}$ | $\eta^{(H)}$ | $\eta^{(T)}$ |
| 5 | 1.1850 | 0.9284 | 1.1711 | – | 0.8374 | – |
| 6 | 1.2547 | 1.0921 | 1.3206 | 1.0879 | 1.2221 | 1.0822 |
| 7 | 1.1578 | 1.2192 | 1.1652 | 1.1532 | 1.1560 | 1.1784 |
| 8 | 1.0593 | 1.1082 | 1.0459 | 1.1017 | 1.0452 | 1.1092 |
| 9 | 0.9132 | 0.7661 | 0.9121 | 0.7477 | 0.9622 | 0.7602 |
| 10 | 0.6253 | 0.3336 | 0.6206 | 0.3278 | 0.6255 | 0.3407 |
| 11 | 0.3676 | 0.2234 | 0.3948 | 0.2147 | 0.3823 | 0.2158 |

## 6. Conclusion

A computational methodology for the optimization of conjugate convective and conductive heat transfer in internally finned ducts was formulated and demonstrated in the earlier sections of this

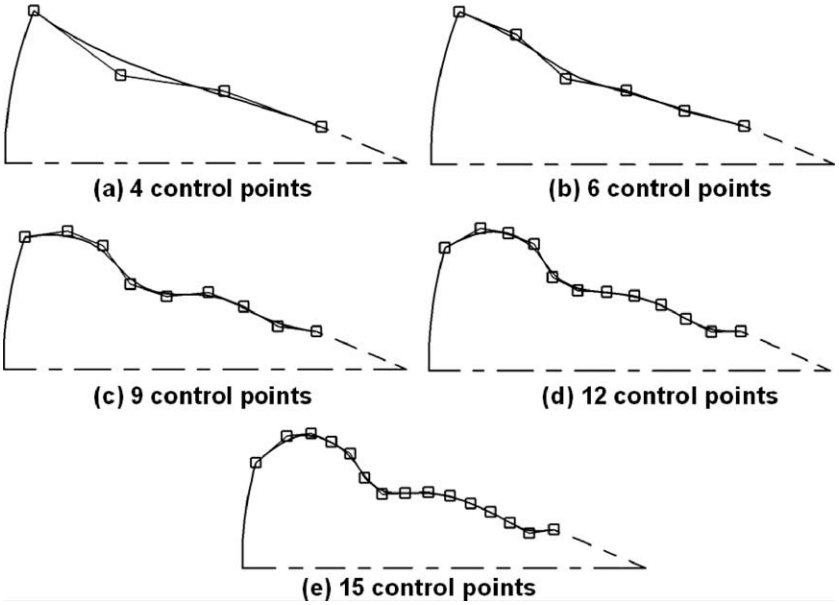


**Fig. 8.** Effect of the number of control points on the optimized fin shape for Case 1 with the number of fins fixed at $n_{fin} = 8$.

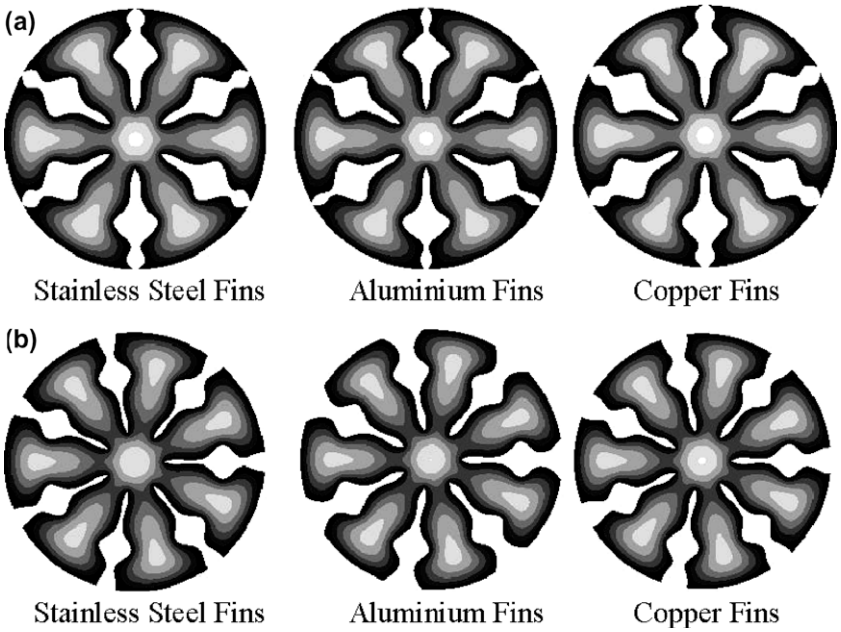


**Fig. 9.** Optimal fin shapes and fully-developed dimensionless axial velocity contours for Case 1: (a) (H) boundary condition and (b) (T) boundary condition.

**Table 2**
Results provided by the optimization methodology for Case 2.

| $n_{fin}$ | Stainless steel | | Aluminium | | Copper | |
|---|---|---|---|---|---|---|
| | $\eta^{(H)}$ | $\eta^{(T)}$ | $\eta^{(H)}$ | $\eta^{(T)}$ | $\eta^{(H)}$ | $\eta^{(T)}$ |
| 7 | 7.0655 | 8.9105 | 7.4590 | 6.7556 | 7.4877 | 8.2802 |
| 8 | 7.6800 | 8.7990 | 7.5813 | 8.7996 | 7.6325 | 8.1858 |
| 9 | 7.1425 | 10.681 | 7.1011 | 10.496 | 7.0760 | 10.614 |
| 10 | 6.2510 | 9.5603 | 6.4299 | 9.5827 | 6.4631 | 9.5480 |
| 12 | 4.3496 | 2.9840 | 4.3766 | 3.0626 | 4.3676 | 3.0671 |
| 14 | 1.8662 | 1.4303 | 1.8572 | 1.4369 | 1.8563 | 1.4217 |
| 16 | 1.0284 | 1.0135 | 1.0237 | 1.0104 | 1.0235 | 1.0168 |

paper. The particular optimization criterion used was the maximization of the thermal performance for a fixed specified value of the pumping power per unit length, but the proposed methodology can be adapted to work with other suitable optimization criteria. The shapes of the internal fins were approximated using non-uniform rational B-splines (NURBS), with the control points as design variables. A two-stage iterative solution methodology was proposed and demonstrated: in the first stage, a control-volume finite element method (CVFEM) and a finite volume method (FVM) are used to solve the so-called *direct* problem, namely, the mathematical models of conjugate convection in the fluid and quasi one-dimensional conduction inside the fins, respectively; in the second stage, an optimization algorithm, based on a gradient approach and inputs from solutions of the aforementioned direct problem, is used to calculate a new geometry of the internally finned duct that moves it towards the desired design; and these two stages are used sequentially and repeatedly until the solution is optimal within a specified tolerance.

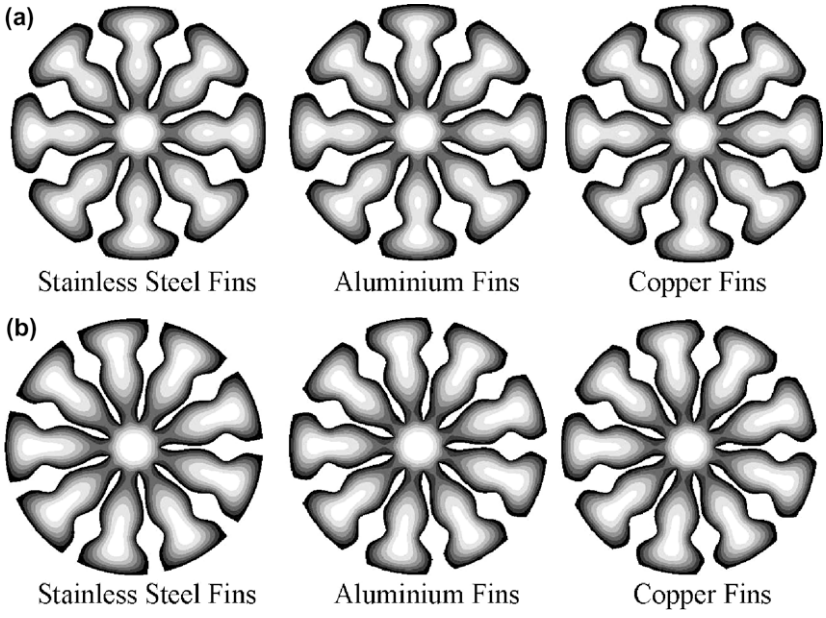


**Fig. 10.** Optimal fin shapes and fully-developed dimensionless axial velocity contours for Case 2: (a) (H) boundary condition and (b) (T) boundary condition.

The proposed overall optimization methodology was demonstrated in the context of steady, fully-developed, laminar forced convection in straight ducts of circular cross-section, with non-twisted, continuous, longitudinal fins. Air was the working fluid, and the fin materials explored were stainless steel, aluminium, and copper. Results pertaining to the maximization of the thermal performance, subject to the constraint of constant pumping power per unit length, were presented and discussed for two baseline cases of the demonstration problem. When the fluid flow in the *baseline* problem is already fairly well distributed in the regions between the fins, as in Case 1 of the demonstration problem, the improvements in thermal performance yielded by the optimized ducts are relatively modest. On the other hand, when the fluid flow in the *baseline* problem is rather poorly distributed, with most of it in the central region of the duct and only relatively low-velocity flow in the regions between the fins, as in Case 2 of the demonstration problem, the optimized ducts provide dramatic improvements in the relative thermal performance.

The proposed computational optimization methodology does not guarantee the absolute optimal solution for each problem, as its gradient-based search method may lock in on a local maximum, should one exist, rather than the absolute maximum. However, it provides a useful way of achieving significant improvements in the relative thermal performance of internally finned ducts, as was shown by the results obtained for the demonstration problem. In the solution of this problem, the gradients required in the optimization algorithm were obtained using direct numerical differentiation of results yielded by the CVFEM and FVM solutions of the intermediate direct problems. To make the proposed methodology viable for the solution of more complex engineering problems, it is recommend that the aforementioned gradients be obtained using either continuous sensitivity equations (CSE) or adjoint methods [25,38,41,61].

## Acknowledgements

Financial sponsorship of this work by the Natural Sciences and Engineering Research Council (NSERC) of Canada, through a research grant to the second author, is gratefully acknowledged. The second author and his current and former students would also like to express their deep gratitude to Professor D.B. Spalding, who has been and continues to be a source of great inspiration to them.

## References

[1] W.M. Kays, A.L. London, Compact Heat Exchangers, third ed., McGraw-Hill, New York, 1984.
[2] J.E. Hesselgreaves, Compact Heat Exchangers: Selection, Design, and Operation, Pergamon, NY, 2001.
[3] R.K. Shah, M.R. Heikal, B. Thonon, P. Tochon, Progress in the numerical analysis of compact heat exchanger surfaces, Adv. Heat Transfer 34 (2001) 363–443.
[4] A.E. Bergles, Some perspectives on enhanced heat transfer – second-generation heat transfer technology, J. Heat Transfer 110 (1988) 1082–1096.
[5] E.M. Sparrow, B.R. Baliga, S.V. Patankar, Heat transfer and fluid flow analysis of interrupted-wall channels, with application to heat exchangers, ASME J. Heat Transfer 99 (1977) 4–11.
[6] S.V. Patankar, C.H. Liu, E.M. Sparrow, Fully developed flow and heat transfer in ducts having streamwise-periodic variations of cross-sectional area, ASME J. Heat Transfer 99 (1977) 180–186.
[7] S.V. Patankar, C. Prakash, An analysis of the effect of plate thickness on laminar flow and heat transfer in interrupted-plate passages, Int. J. Heat Mass Transfer 24 (1981) 1801–1810.
[8] K.M. Kelkar, S.V. Patankar, Numerical prediction of heat transfer and fluid flow in rectangular offset-fin arrays, Numer. Heat Transfer A 15 (1989) 149–164.
[9] C.H. Amon, D. Majumdar, C.V. Herman, F. Mayinger, B.B. Mikic, D. Sekulic, Numerical and experimental studies of self-sustained oscillatory flows in communicating channels, Int. J. Heat Mass Transfer 35 (1992) 3115–3129.
[10] K. Suzuki, G.N. Xi, K. Inaoka, Y. Hagiwara, Mechanism of heat transfer enhancement due to self-sustained oscillation for an in-line fin array, Int. J. Heat Mass Transfer 37 (Suppl. 1) (1994) 83–96.
[11] L.W. Zhang, S. Balachandar, D.K. Tafti, F.M. Najjar, Heat transfer enhancement mechanisms in inline and staggered parallel-plate fin heat exchangers, Int. J. Heat Mass Transfer 40 (1997) 2307–2325.
[12] S. Acharya, T. Myrum, S. Sinha, X. Qiu, Developing and periodically developed flow, temperature and heat transfer in a ribbed duct, Int. J. Heat Mass Transfer 40 (1997) 461–480.
[13] N.C. DeJong, L.W. Zhang, A.M. Jacobi, S. Balachandar, D.K. Tafti, A complementary experimental and numerical study of the flow and heat transfer in offset strip-fin heat exchangers, ASME J. Heat Transfer 120 (1998) 690–698.
[14] A. Saidi, B. Sundén, A numerical investigation of heat transfer enhancement in offset strip fin heat exchangers in self-sustained oscillatory flows, Int. J. Numer. Methods Heat Fluid Flow 11 (2001) 699–717.
[15] A. Lamoureux, B.R. Baliga, Temporally- and spatially-periodic laminar flow and heat transfer in staggered-plate arrays, in: Proc. ASME-JSME Thermal Engineering Summer Heat Transfer Conference (HT2007), Paper HT2007-32679, Vancouver, British Columbia, Canada, July 8–12, 2007, pp. 1–10.
[16] J.H. Masliyah, K. Nandkumar, Heat transfer in internally finned tubes, ASME J. Heat Transfer 98 (1976) 257–261.
[17] H.M. Soliman, T.S. Chau, A.C. Trupp, Analysis of laminar heat transfer in internally finned tubes with uniform outside wall temperature, ASME J. Heat Transfer 102 (1980) 598–604.
[18] S.V. Patankar, M. Ivanovic, E.M. Sparrow, Analysis of turbulent flow and heat transfer in internally finned tubes and annuli, ASME J. Heat Transfer 101 (1979) 29–37.
[19] R.L. Webb, M.J. Scott, A parametric analysis of the performance of internally finned tubes for heat exchanger application, ASME J. Heat Transfer 102 (1980) 38–43.
[20] B.R. Baliga, R.R. Azrak, Laminar fully developed flow and heat transfer in triangular plate-fin ducts, ASME J. Heat Transfer 108 (1986) 24–32.
[21] Y. Zhang, A. Faghri, Heat transfer enhancement in latent heat thermal energy storage system by using the internally finned tube, Int. J. Heat Mass Transfer 39 (1996) 3165–3173.
[22] F.C. Chou, J.R. Lukes, C.L. Tien, Heat transfer enhancement by fins in the microscale regime, ASME J. Heat Transfer 121 (1999) 972–977.
[23] O. Pironneau, Optimal Shape Design for Elliptic Systems, Springer Series in Computational Physics, Springer-Verlag, New York, 1994.
[24] S.S. Rao, Engineering Optimization: Theory and Practice, third ed., John Wiley & Sons, Inc., New York, 1996.
[25] A. Jameson, L. Martinelli, N.A. Pierce, Optimum aerodynamic design using the Navier–Stokes equations, Theor. Comput. Fluid Dyn. 10 (1998) 213–237.
[26] G. Fabbri, A genetic algorithm for fin profile optimization, Int. J. Heat Mass Transfer 40 (1997) 2165–2172.
[27] G. Fabbri, Heat transfer optimization in finned annular ducts under laminar-flow conditions, Heat Transfer Eng. 19 (1998) 42–54.
[28] A. Bejan, Shape and Structure, from Engineering to Nature, Cambridge University Press, Cambridge, UK, 2000.
[29] K. Deb, Multi-Objective Optimization using Evolutionary Algorithms, John Wiley, West Sussex, England, 2001.
[30] G.C. Onwubolu, B.V. Babu, in: New Optimization Techniques in Engineering, Studies in Fuzziness and Soft Computing, vol. 141, Springer-Verlag, Berlin, 2004.
[31] B. Mohammadi, O. Pironneau, Shape optimization in fluid mechanics, Annu. Rev. Fluid Mech. 36 (2004) 255–279.
[32] F. Bobaru, S. Rachakonda, Optimal shape profiles for cooling fins of high and low conductivity, Int. J. Heat Mass Transfer 47 (2004) 4953–4966.
[33] F. Bobaru, S. Rachakonda, Boundary layer in shape optimization of convective fins using a meshfree approach, Int. J. Numer. Methods Eng. 60 (2004) 1215–1236.
[34] A. Bejan, S. Lorente, Constructal theory of generation of configuration in nature and engineering, J. Appl. Phys. 100 (2006) 041301, 1–27.
[35] T. Dias Jr., L.F. Milanez, Optimal location of heat sources on a vertical wall with natural convection through genetic algorithms, Int. J. Heat Mass Transfer 49 (2006) 2090–2096.
[36] R. Hilbert, G. Janiga, R. Baron, D. Thévenin, Multi-objective shape optimization of a heat exchanger using parallel genetic algorithms, Int. J. Heat Mass Transfer 49 (2006) 2567–2577.
[37] G. Lorenzini, L.A.O. Rocha, Constructal design of Y-shaped assembly of fins, Int. J. Heat Mass Transfer 49 (2006) 4552–4557.
[38] R. Duvigneau, D. Pelletier, J. Borggaard, An improved continuous sensitivity equation method for optimal shape design in mixed convection, Numer. Heat Transfer B 50 (2006) 1–24.
[39] G. Janiga, A few illustrative examples of CFD-based optimization, in: D. Thévenin, G. Janiga (Eds.), Optimization and Computational Fluid Dynamics, Springer-Verlag, Berlin, 2008, pp. 17–59 (Chapter 2).
[40] M. Tye-Gingras, L. Gosselin, Thermal resistance minimization of a fin-and-porous-medium heat sink with evolutionary algorithm, Numer. Heat Transfer A 54 (2008) 349–366.
[41] K. Shinohara, H. Okuda, S. Ito, N. Nakajima, M. Ida, Shape optimization using adjoint variable method for reducing drag in stokes flow, Int. J. Numer. Methods Fluids (2008), 10.1002/fld.1677.
[42] A.K. da Silva, L. Gosselin, Evolutionary placement of discrete heaters in forced convection, Numer. Heat Transfer A 54 (2008) 20–33.
[43] K. Kurpisz, A.J. Nowak, Inverse Thermal Problems, Computational Mechanics Publications, Billerica, MA, US, 1995.
[44] M.N. Özisik, H.R.B. Orlande, Inverse Heat Transfer – Fundamentals and Applications, Taylor & Francis, New York, 2000.
[45] A. Ashrafizadeh, G.D. Raithby, G.D. Stubley, Direct design of shape, Numer. Heat Transfer B 41 (2002) 501–520.
[46] A. Ashrafizadeh, G.D. Raithby, G.D. Stubley, Direct design of ducts, ASME J. Fluids Eng. 125 (2003) 158–165.

[47] A. Bar-Cohen, Fin thickness for an optimized natural convection array of rectangular fins, ASME J. Heat Transfer 101 (1979) 564–566.
[48] A. Bar-Cohen, W.M. Rohsenow, Thermally optimum spacing of vertical, naturally convection cooled parallel plates, ASME J. Heat Transfer 106 (1984) 116–123.
[49] P. Razelos, R.N. Krikkis, On the optimum thermal design of individual longitudinal fins with rectangular profile, Int. Commun. Heat Mass Transfer 30 (2003) 349–358.
[50] Y. Tsukamoto, Y. Seguchi, Shape optimization problem for minimum volume fin, Heat Transfer Jpn. Res. 13 (1984) 1–19.
[51] E. Lorenzini, M. Spiga, G. Fabbri, A polynomial fin profile optimization, Int. J. Heat Technol. 12 (1994) 137–144.
[52] G. Fabbri, Heat transfer optimization in internally finned tubes under laminar flow conditions, Int. J. Heat Mass Transfer 41 (1998) 1243–1253.
[53] G. Fabbri, Optimization of heat transfer through finned dissipators cooled by laminar flow, Int. J. Heat Fluid Flow 19 (1998) 644–654.
[54] O. Soto, R. Löhner, CFD shape optimization using an incomplete-gradient adjoint formulation, Int. J. Numer. Methods Eng. 51 (2001) 735–753.
[55] L. Piegl, W. Tiller, The NURBS book, second ed., Monographs in Visual Communication, Springer-Verlag, Berlin, 1997.
[56] B.R. Baliga, S.V. Patankar, A new finite-element formulation for convection–diffusion problems, Numer. Heat Transfer 3 (1980) 393–409.
[57] B.R. Baliga, N. Atabaki, Control-volume-based finite-difference and finite-element methods, in: W.J. Minkowycz, E.M. Sparrow, J.Y. Murthy (Eds.), Handbook of Numerical Heat Transfer, second ed., Wiley, New York, 2006, pp. 191–224 (Chapter 6).
[58] D.B. Spalding, A novel finite-difference formulation for differential expressions involving both first and second derivatives, Int. J. Numer. Methods Eng. 4 (1972) 551–559.
[59] S.V. Patankar, D.B. Spalding, A calculation procedure for heat, mass and momentum transfer in three-dimensional parabolic flows, Int. J. Heat Mass Transfer 15 (1972) 1787–1806.
[60] S.V. Patankar, Numerical Heat Transfer and Fluid Flow, Taylor & Francis, New York, 1980.
[61] K. Dems, Z. Mroz, Sensitivity analysis and optimal design of external boundaries and interfaces for heat conduction systems, J. Therm. Stresses 21 (1998) 461–488.
[62] E.R.G. Eckert, R.M. Drake, Analysis of Heat and Mass Transfer, McGraw-Hill, New York, 1971.
[63] F.P. Incropera, D.P. DeWitt, Introduction to Heat Transfer, fourth ed., Wiley, New York, 2002.
[64] W.M. Kays, M.E. Crawford, Convective Heat and Mass Transfer, third ed., McGraw-Hill, New York, 1993.
[65] R.K. Shah, A.L. London, Laminar Flow Forced Convection in Ducts, Supplement 1, Advances in Heat Transfer, Academic Press, New York, 1978.
[66] E.M. Sparrow, S.V. Patankar, Relationships among boundary conditions and Nusselt numbers for thermally developed duct flows, ASME J. Heat Transfer 99 (1977) 483–485.